Investigating the chemo-preventive role of noscapine in lung carcinoma via therapeutic targeting of human aurora kinase B

Saba Noor
Jamia Millia Islamia
Khursheed Ul Islam
Jawahar Lal Nehru Medical College, Aligarh Muslim University
Arunabh Choudhury
Jamia Millia Islamia
Mohd. Yousuf
Jamia Millia Islamia
Ali Raza
University College of Medical Sciences
Mohammad Ahmad Ansari
Jamia Millia Islamia
Anam Ashraf
Jamia Millia Islamia
Afzal Hussain
King Saud University
Md. Imtaiyaz Hassan
mihassan@jmi.ac.in

Jamia Millia Islamia

Research Article

Keywords: Lung cancer, human aurora kinase B, Natural products, Noscapine, Drug discovery, MD simulation studies

Posted Date: February 28th, 2024

DOI: https://doi.org/10.21203/rs.3.rs-3962159/v1

Additional Declarations: No competing interests reported.

Abstract

Lung carcinoma is the major contributor to global cancer incidence and one of the leading causes of cancer-related mortality worldwide. Irregularities in signal transduction events, driver genetic alterations, and mutated regulatory genes trigger cancer development and progression. Selective targeting of molecular modulators has substantially revolutionized cancer treatment strategies with improvised efficacy. The aurora kinase B (AURKB) is a key component of the chromosomal passenger complex and is primarily involved in lung cancer pathogenesis. Since AURKB is an attractive therapeutic target, the design and development of its potential inhibitors is an attractive strategy. In this study, noscapine, a benzylisoquinoline alkaloid, was selected and validated as a potential inhibitor of AURKB using integrated computational, spectroscopic, and cell-based assays. Molecular docking analysis showed noscapine occupies the substrate-binding pocket of AURKB with strong binding affinity. Subsequently, MD simulation studies confirmed the formation of a stable AURKB-noscapine complex with non-significant alteration in various trajectories, including RMSD, RMSF, *Rg*, and SASA. These findings were further experimentally validated through fluorescence binding studies. In addition, dose-dependent noscapine treatment significantly attenuated recombinant AURKB activity with an IC_{50} value of 26.6 μM. Cell viability studies conducted on A549 cells and HEK293 cells revealed significant cytotoxic features of noscapine on A549 cells. Furthermore, Annexin-PI staining validated that noscapine triggered apoptosis in lung cancer cells, possibly via an intrinsic pathway. Our findings indicate that noscapine-based tandem AURKB inhibition can be implicated as a potential therapeutic strategy in lung cancer treatment and can also provide a novel scaffold for developing next-generation AURKB-specific inhibitors.

1. Introduction

Protein kinases are abundantly expressed intracellularly, crucial in signal transduction *via* phosphorylation of several proteins. Altered expression of protein kinases or genetic mutation underlies the pathogenesis of several human diseases, including cancer [1]. Due to their critical play in signaling mechanisms that drive cell growth, proliferation, and survival, protein kinases are essential therapeutic targets in cancer therapy. Aurora kinases (AURKA, AURKB, and AURKC) belong to the Serine/Threonine class of kinases, with an imperative role in cell mitosis and meiosis [2]. AURKA and AURKB maintain chromosomal integrity in mitosis, whereas AURKC regulates gametogenesis. These three members exhibit high structural homology in mammalian cells. AURKB is a crucial regulator of chromosomal passenger complex (CPC) driving spindle assembly and ensures correct chromosomal segregation by phosphorylating CPC complex units, including survivin, boreal, and INCEP [3]. In addition, AURKB also phosphorylates histone 3 [4] and attenuates the transcriptional activity of the p53 protein [5]. AURKB also regulates the spindle assembly checkpoint proteins Bub, SGO1, Mps1, and Mad, favoring cytokinesis [6]. Defects in mitotic checkpoints deformed chromosomal accumulation and cohesion modulated by abnormal AURKB may lead to aneuploidy and genetic instability.

Studies have reported that small molecule-based targeted AURKB inhibition influences microtubule assembly and triggers chromosomal segregation disorders, including human malignancies of the

prostate, lung, breast, and colon [7]. Emerging evidence from *in-vitro* and *in-vivo* studies suggests that AURKB attenuation could potentiate the effect of conventional chemotherapies implicated in cancer treatment [8, 9]. With so many diverse and integral roles in cellular division, AURKB exhibits oncogenic potential and can be a promising target in cancer therapeutics. Several small molecules designed against AURKB have been studied, but none have been launched on the market and are still in pre-clinical and clinical phases. Among synthetic AURKB inhibitors, VX-680, MK-0457, or Tozasertib exhibits significant anti-cancer potential and is in the advanced stages of clinical trials. VX-680 impedes AURKB-based histone 3 phosphorylation, delays mitotic cell progression, and triggers polyploidy and apoptosis in cancer cells [10].

Recently, a significant shift has been detected in screening bioactive natural compounds as potent kinase inhibitors in cancer therapeutics. Dietary polyphenolic derivatives possess significant anti-oxidant, anti-inflammatory, and anti-cancer potential and have been extensively studied in various cancer models. These polyphenols are identified as solid human kinase inhibitors, including cyclin-dependent kinase (CDK) [11], Janus kinases (JAK) [12], rapidly accelerated fibrosarcoma (Raf), mitogen-activated protein kinase (MAPK), and SphK1 [13]. Anti-cancer molecules from natural sources such as vinblastine and taxol have shown significant tumor regression in cancer patients [14].

Noscapine is a benzylisoquinoline alkaloid isolated from the opium poppy (*Papaver somniferum L.)* with anti-tussive properties and negligible euphoric and addictive side effects [15]. In a recent decade, noscapine has been reported to exert several pharmacological roles against cancer, diabetes, cardiovascular ailments, and other metabolic diseases. Exposure to noscapine inhibited the progression of ovarian cancer, breast cancer, lung cancer, and prostate cancer, thereby preventing cancer development [16]. Noscapine has been used in combinational therapy with other anti-cancer drugs, such as doxorubicin, against triple-negative breast cancer. In combination, noscapine synergized strongly, enhancing cancer cell apoptosis [17]. Similarly, noscapine in conjugation with gemcitabine regressed non-small lung cancer by enhancing mitotic arrest [18]. This compound has recently been considered an anti-mitotic agent affecting important signaling cascades in cancer cells. Noscapine is regarded as a pleiotropic kinase inhibitor and has been reported to attenuate CDK4/6 [19], epidermal growth receptor tyrosine kinase [20], and Iκ-B kinase [21].

Based on previous studies, noscapine has structural similarity with colchicine and is expected to bind tubulin, leading to confirmational changes altering microtubule assembly, eventually arresting mitosis in the G2/M transition phase [22]. Studies have reported that noscapine and its structural derivatives can reduce microtubule dynamics by increasing microtubule stopping time [23]. Since altered AURKB leads to deformed microtubule assembly and subsequent mitosis of aneuploid cells, targeted AURKB inhibition might prevent the formation of cells with altered genomic content. Therefore, based on the anti-cancer properties of noscapine and its role as a potential kinase inhibitor, we postulate that noscapine can be exploited in cancer therapeutics as an AUKRB inhibitor.

Through *in-silico* approaches, we have defined the binding mechanism of noscapine with AURKB, which was later confirmed by fluorescence studies and kinase inhibition assay. We further investigated noscapine's anti-cancer and anti-proliferative potential on lung cancer cell lines. Our findings report that noscapine binds efficiently within the kinase domain of AURKB and significantly inhibits catalytic activity. Thus, a noscapine scaffold can be implemented to design and develop novel AURKB inhibitors against lung cancer.

2. Material and Methods

2.1. Chemical reagents and plasmids

The pET28a^{+} plasmid containing recombinant AURKB gene with 6X-histidine tag added to the N-terminal was procured from Biomatik®. DH5-α and BL21(DE3) cells for transformation were obtained from Invitrogen (USA). Nickel-NTA columns for protein purification were purchased from GE Healthcare (Uppsala, Sweden). Chemicals including N-Lauryl Sarcosine, Tris, Isopropyl β- d-1-thiogalactopyranoside (IPTG), 3- [4, 5-dimethylthiazol-2-yl]-2,5-diphenyl tetrazolium bromide (MTT) dye, and noscapine were obtained from Sigma Aldrich. The lung cancer cell line, human alveolar basal epithelial cells (A549), and human embryonic kidney cells (HEK293) were ordered from the National Centre for Cell Sciences, Pune, India. For cell culture, Dulbecco's modified eagle medium (DMEM), fetal bovine serum (FBS), PenStrep, phosphate buffer saline (PBS), and trypsin enzyme were purchased from Gibco technologies, Thermo-Fischer Scientific (USA). Isolation of plasmid, preparation of competent cells, and transformation were done using standard procedures.

2.2. Physiochemical and pharmacokinetic properties of noscapine

Natural flavonoids, including noscapine, are reported to exhibit anti-oncogenic, anti-oxidant, and anti-inflammatory. The physicochemical properties, drug likeliness, lipophilicity, and pharmacokinetic profile of noscapine were determined using SwissADME software. Noscapine was further analyzed based on Lipinski's Rule, and further, ADME properties were predicted to support drug likeliness. In addition, prediction of activity spectra of substances (PASS) analysis was conducted on noscapine to assess and validate its pharmacological characteristics. Based on the structure-activity relationship, PASS tools predict pharmacological actions, biological benefits, interactions with signaling cascade members, including enzymes, transporters, and other proteins, and potential roles in cancer therapeutics. Compounds depicting P*a* > P*i* are considered probable actives.

2.3. Molecular Docking

Binding affinity and detailed interactions were elucidated with molecular docking of noscapine with AURKB. 3D atomic coordinates of AURKB (4AF3) co-crystalized with VX-680 were downloaded from RCBS (www.rcsb.org) and processed in Pymod 2.0 software for structure remodeling. In addition, the 3D structure of noscapine was obtained from the PubChem database and processed in ChemBiodraw Ultra

12.0. SPDVB and MGL tools were utilized for structure preprocessing and energy minimization. The docking of AURKB with noscapine was performed using InstaDock 2.0 to elucidate binding energy, ligand efficiency, and protein-ligand interaction [24]. The binding affinities between the ligand and protein were calculated using the QuickVina-W. PyMol viewer and BIOVIA/Discovery Studio 2017R2 platforms were used for computational analysis and visualization of interacting patterns of docked structures.

2.4. MD simulation studies

MD simulation studies were conducted to comprehend the changes in conformational dynamics of AURKB upon noscapine binding through *in-silico* approaches. The stability and conformational dynamics of the AURKB-noscapine docked complex were measured through 100 ns simulation using GROMACS v5.5.1 software. Two systems of native AURKB and AURKB-noscapine were prepared and soaked in a cubic box with a 10 Å distance from the protein, incorporating the simple point-charge (SPC16) water model. Solvated systems were subjected to 1500 steps of the steepest descent method for energy minimization to negate potential steric hindrances. A two-step equilibration was performed for 1000 ps involving the periodic boundary conditions. Subsequently, a simulation of 100 ns was conducted for each system. Comparative data, including RMSD, RMSF, Rg, and SASA, was computed on MD trajectories using the GMX tool. The resulting trajectories were analyzed using *gmxenergy, gmxrms, gmxconfirms, gmxrmsf, gmx gyrate, make_ndx,gmx hbond*, *gmxdo_dssp*, and *gmx sasa* utilities of GROMACS. The possibility of ligand interactions with important residues of protein was calculated during the whole simulation period. All graphs were prepared using QtGrace software.

2.5. AURKB expression and purification

AURKB transformed BL21(DE3) was grown overnight in Luria Bertani broth at 180 rpm with added kanamycin (50 μg/mL). Subsequently, secondary cultures were inoculated with 1% primary culture, grown for a few hours, and induced with 1 mM IPTG. Post-induction cells were pelleted at 5,500 rpm and suspended in lysis buffer (Tris-50 mM, NaCl-200 mM, pH 7.5, 1% Triton X, 2% Glycerol, 1 mM PMSF, 0.5 mM TCEP). The resuspended pellet was further sonicated in a cold chamber for 15 mins (20 sec on/off) followed by centrifugation at 10,000 rpm for 30 mins. AURKB protein was checked both in the supernatant and cell pellet with SDS-PAGE. The cell pellet was again thoroughly mixed in a lysis buffer (Tris-50 mM, NaCl-200 mM), and inclusion bodies (IBs) were prepared by repeated washing with double distilled water followed by centrifugation. After washing, IBs were stored at -20 ºC for further use.

The protein was purified by following our published protocol [25]. In summary, IBs (1mL) were solubilized in a solubilization buffer (Tris-50 mM, NaCl-200 mM, pH 7.5) containing 0.5% N-Lauryl sarcosine in a cold chamber until a clear solution was obtained. Ni-NTA chromatography column was washed with milli-Q water and equilibrated with equilibrating buffer (Tris-50 mM, NaCl-200 mM, pH 7.5). A clear solution of solubilized IBs after centrifugation was loaded into the equilibrated Ni-NTA column in a cold chamber. The column was washed with 10 mM imidazole to remove impurities, and His-tag AURKB protein was eluted in 50 mM imidazole solution prepared in Tris-50 mM, NaCl-200 mM buffer. Later, the Ni-NTA column was washed with 1M imidazole solution and stored in milli-Q water at 4^0C. Eluted samples were

analyzed with SDS-PAGE to elucidate protein purity. The eluted protein was subjected to overnight dialysis with continuous stirring at 4^0C in Tris-25 mM, NaCl-100 mM buffer with intermittent buffer changes for complete refolding. UV-Spectroscopy (Jasco-V-660) of dialyzed AURKB protein was conducted to assess the concentration and folding to the native state.

2.6. Fluorescence measurements

To validate the findings of molecular docking and binding affinities of noscapine with AURKB, a fluorescence spectroscopic experiment was done on a Jasco Spectrofluorometer (FP-6200, Jasco, Japan) in a 5 mm quartz cuvette. The stock solution of noscapine (50 mM) was prepared in dimethyl sulphoxide (DMSO), and a working solution (1 mM) was made in Tris-50 mM NaCl-200 mM buffer. Purified AURKB (4 μM) was allowed to interact with an increasing concentration of noscapine (1–50 μM) and mixed thoroughly. AURKB was excited at a wavelength of 280 nm, and intrinsic fluorescence emission spectra were monitored in the 300–400 nm range. The gradual changes in fluorescence intensity were noted upon an increase in noscapine concentration. Experiments were performed in triplicates, and average data was plotted. An inverse co-relationship between fluorescence intensity and increasing noscapine concentration was implemented in deducing kinetic parameters using the Stern-Volmer equation. The binding affinity constant of the AURKB-noscapine complex (*Ka*) was also calculated.

2.7. Enzyme inhibition assay

An ATPase assay was conducted following previous methods to determine the impact of noscapine on AURKB activity [26]. An increasing concentration of noscapine (0-100 μM) was used to interact with purified AURKB (4 μM) for 45 mins at 25^0C. Further, the formed complex was incubated with 200 μM ATP for 30 mins at 37^0C. The reaction was halted by adding BIOMOL® GREEN reagent to the reaction mixture. The changes in color intensity at 620 nm were measured using an ELISA plate reader (BioRad)

2.8. Cell culture and viability assay

Cytotoxic and anti-proliferative effects of noscapine on lung cancer cell line (A549) were assessed with MTT assay. A549 cells were maintained in DMEM media supplemented with 10% heat inactivated filtered FBS and 1% PenStrep antibiotic cocktail in a humified 5% CO_2 incubator maintained at 37^0C. HEK293 cells were used as normal controls in this study. The cytotoxic potential of noscapine on A549 and HEK293 cells was monitored using standard MTT assay protocol as described previously [27, 28]. Cells were seeded in 96 well plates 8000–9000 cells and allowed to grow for 24 hrs at 37^0C. In a separate set of experiments, both cell lines were treated with increasing concentrations of noscapine (0-250 μM) in a total reaction volume of 200 μL and later kept for 48 hrs in a humified CO_2 incubator, 37 ^{0}C. The treated cells were harvested and processed for cell viability studies using an MTT assay. The media was discarded, and cells were washed with 1X PBS (pH 7.4). A stock of MTT dye (5 mg/mL) was prepared in DMEM media, added to each, and incubated for 4–5 hrs at 37^0C in a CO_2 incubator. Subsequently, the supernatant was removed, and formazan crystals formed were dissolved in 100 μL DMSO solution. The

absorbance of the reaction was recorded using an ELISA plate reader (BioRad) at 570 nm. The percentage cell viability was calculated and plotted as a function of increasing noscapine concentration.

2.9. Cell apoptosis analysis

The apoptotic potential of noscapine on A549 cells was elucidated with Annexin-V/PI staining. Briefly, A549 cells were treated with an IC_{50} dose of noscapine for 48 hrs at 37^0C in a CO_2 incubator, whereas untreated cells were treated with media only. Following treatment, cells from both groups were trypsinized and later harvested. Harvested cells were washed three times with 1X PBS and stained with FITC-labelled Annexin-V using FITC- Annexin-V kit **(name)** per manufacturer protocols. Collected cells were resuspended in 100 μL of 1X Annexin-V binding buffer, containing 5 μL each Annexin-V-FITC and PI alone and in combination with both. Samples were incubated in the dark for 15 minutes at room temperature. Later, 400 μL of 1X binding buffer was added to stop the reaction, and samples were visualized using flow cytometry (FACS Aria III; Becton Dickinson, CA, USA), and data were analyzed using FlowJo software (FlowJo LLC, USA).

2.10. DAPI staining

A549 cells were seeded on poly L lysine-coated coverslips at a density of 0.1×10^6 cells per well of a 12-well cell culture plate. Cells were allowed to grow in DMEM with 10% FBS inside a CO_2 incubator, maintaining 37^0C, 5% CO_2, and 90% humidity. At 60–70% confluency, cells were treated with an IC_{50} dose of noscapine and a positive control staurosporine at a concentration of 1μM. Cells were allowed to grow under drug treatment for 48 hrs. After incubation, cells were harvested for DAPI staining. DAPI staining was performed as described previously [29] with slight modification. Briefly, cells were washed with 1X PBS and fixed in 4% paraformaldehyde for 20 mins. After the aspiration of fixing solution, cells were washed (3X) with 1XPBS. Cells were further incubated with nucleus staining dye, 4',6-diamidino-2-phenylindole (DAPI) at a concentration of 1μg/mL for 5–10 mins at room temperature. After washing the cells with PBS, coverslips were mounted onto a glass coverslip containing an antifade mounting medium VECTASHIELD and observed under a Zeiss Axio observer 7 immunofluorescence microscope.

2.11. Wound healing assay

Wound healing assay is a non-expensive and highly reproducible technique to determine cell migration *in vitro.* The ability of noscapine to inhibit cancer cell migration on A549 cells was studied using the wound healing assay mentioned in previous literature [30]. In brief, A549 cells were grown in a six-well plate, and at 60–70% confluency, a scratch was created precisely by scraping the cell monolayer using the tip of a 200 μL micropipette tip. The detached cells were gently washed off, and fresh media was added. Cells were then treated with an IC_{50} dose of noscapine for 48 hrs at 37^0C in a CO_2 incubator. Post-treatment cells were then fixed in 4% paraformaldehyde and visualized on an inverted phase contrast microscope.

3. Results

3.1. Physicochemical and pharmacokinetic properties of noscapine

Physicochemical descriptors, ADME parameters, drug likeliness, and pharmacokinetic parameters were computed for noscapine, suggesting the drug-likeness of noscapine, which can be implicated in AURKB-targeted cancer therapy after in-depth validation and optimizations (Table 1). ADME properties and pharmacokinetic profile of noscapine further supported its drug likeliness. Noscapine has a high GI absorption profile, indicating excellent noscapine absorption when administered orally. Also, noscapine is not a substrate of CYP2C9, CYP2D6, and P-glycoprotein that predicts a higher plasma concentration of noscapine upon intake as it can skip Phase-I metabolizing enzymes. The structural features of noscapine present no violation of Lipinski's rule of five that indicates a high drug likeliness. Similarly, several other ADMET parameters support drug-like properties of noscapine, and a slight modification in the structure might lead to the development of excellent drug derivatives. The findings of PASS analysis based on the structure-activity relationship further supported the imperative role of noscapine in attenuating and halting the causation and progression of various cancers (Table 2).

Table 1
Physiochemical and pharmacokinetic properties of Noscapine

S. No.	Physiochemical Parameters	Value
1.	Molecular formula	$C_{22}H_{23}NO_7$
2.	Molecular weight	413.42 g/mol
3.	Number of heavy atoms	30
4.	Rotatable bonds	4
5.	Hydrogen acceptor	8
6.	Hydrogen donor	0
7.	Molar refractivity	109.8
8.	TPSA	75.6 $Å^2$
Lipophilicity		
1	iLOGP$_{o/w}$ *(iLOGP)*	3.59
2.	iLOGP$_{o/w}$ *(XLOGP3)*	2.71
3.	iLOGP$_{o/w}$ *(WLOGP)*	1.85
4.	iLOGP$_{o/w}$ *(MLOGP)*	1.69
5.	iLOGP$_{o/w}$ *(SILICOS-IT)*	3.20
Drug likeliness and medicinal chemistry		
1.	Lipinski violations	0
2.	PAINS	0
3.	Ghose	Yes
4.	Bioavailability score	0.55
5.	Volume of Distribution (logL/kg)	0.43
6.	Synthetic accessibility	4.31
7.	Leadlikeness	No; 1 violation: MW > 350
Pharmacokinetic parameters		
1.	GI absorption (%)	95.2%
2.	BBB permeability (log BB)	-0.594
3.	CYP1A2 inhibitor	No

S. No.	Physiochemical Parameters	Value
4.	CYP2D6 inhibitor	Yes
5.	CYP2C9 inhibitor	Yes
6.	P-gp substrate	No
7.	Hepatotoxicity	No
8.	AMES toxicity	No
9.	Skin sensitization	No
10.	Log *Kp* (skin permeation)	-6.90 cm/s

Table 2
Prediction of activity spectra for substances (PASS) of selected polyphenols

Compound	Pa	Pi	Activity
Noscapine	0.706	0.014	Apoptosis agonist
	0.655	0.034	Anti-neoplastic
	0.614	0.005	Anti-mitotic
	0.545	0.004	Anti-neoplastic alkaloid
	0.479	0.019	Anti-neoplastic lung cancer
	0.343	0.009	Antineoplastic (squamous cell carcinoma)
	0.339	0.004	Antineoplastic (breast cancer)
	0.346	0.073	MMP9 expression inhibitor

3.2. Molecular docking of noscapine with AURKB

To comprehend the protein-ligand interactions, molecular docking of AURKB with noscapine was conducted to find interacting amino acid residues, bound conformations, binding energies, and intermolecular distances between AURKB and potential amino acids. Molecular docking results revealed that noscapine binds with an active pocket of AURKB with a binding affinity of -7.4 kcal/mol and showed several potential and strong interactions with the binding pocket residues. The binding mode of noscapine was predicted based on the highest binding affinity of noscapine (-7.4 kcal/mol) with AURKB. It was observed that noscapine occupied the ATP-binding region, and this binding could perhaps competitively inhibit substrate accessibility of AURKB, eventually causing enzyme inhibition.

The AURKB-noscapine complex is stabilized by several non-covalent interactions, including hydrogen bonds, Pi-sigma, van der Wall, and Pi-alkyl interactions (Fig. 1). Noscapine showed closed interactions of major ATP binding domain residues, including Phe88, Gly89, Asn90, Lys106, Leu108, and Phe109. Several spatial arrangements within the AURKB-noscapine complex were also driven by other favorable

interactions besides H-bonding and facilitated by Gln112, Ile113, Glu116, Val118, Phe219, Gly220, Trp221, and His224. Moreover, the surface representations of the docked complex also indicate that noscapine occupies the internal core cavity of AURKB with strong affinity (Fig. 1).

3.3. Structural dynamics study of AURKB-noscapine complex

MD simulation studies were conducted to gain information on atomic motions in native protein and upon ligand binding. MD is a simulation tool that asses structural dynamics and thermodynamical features of molecular systems, including protein molecules. The stability of native protein upon binding with noscapine was determined in a water model. The GROMOS 54A7 force field was used, and free AURKB, AURKB- noscapine was simulated for 100 nanoseconds. Secondary structure changes in AURKB structure upon ligand binding was also analyzed.

Alteration in structural dynamics of protein molecules upon ligand binding alleviates biological functions. RMSD calculation assesses the changes in protein conformation and stability on ligand interaction. Here, the average RMSD values of native AURKB and AURKB-Noscapine complex were found to be 0.44 nm and 0.43 nm, respectively. Within the presented MD simulation period, the obtained RMSD trajectories depicted non-significant fluctuations in complex AURKB throughout the simulation period. These findings indicate the formation of a stable complex upon ligand binding. All the above findings suggest preferential binding of noscapine within the active pocket of AURKB (Fig. 2A).

Further analysis of the local structure flexibility of protein, the per residue RMSF profile was estimated for native and complexed AURKB. The flexibility criterion provides information on the contribution of individual protein residues in structural fluctuations within the complex. Residual fluctuations of free AURKB and upon noscapine binding during simulation were plotted as a function of residue number. RMSF plot evaluates the time evolution of the average deviation for each residue from its reference point within the minimized starting structures. The average RMSF values of free AURKB and complexed with noscapine were 0.16 nm and 0.21 nm, respectively. The RMSF plot showed higher fluctuations between residues 225 and 250 of the AURKB- noscapine complex due to enhanced flexibility in the loop regions. RMSF values showed a negligible difference but achieved stability. Findings showed that both systems showed synchronized RMSF patterns throughout the simulation process, indicating ligand stability in the protein pocket (Fig. 2B).

Rg was monitored throughout MD trajectories for 100 ns to gain deeper insights into complex stability. *Rg* is the mass-weighted RMSD for a group of atoms relative to the center of mass of the protein molecule. This parameter depicts biological systems' global stability/compactness where low average *Rg* values indicate enhanced stability. The average *Rg* values of free and complexed AURKB within the study were 1.94 nm and 2.09 nm, respectively. *Rg* data suggested slightly reduced compactness in AURKB structure upon noscapine binding compared to native. This deviation might occur due to the initial positioning of

the noscapine within the binding pocket of AURKB. However, the *Rg* tones of both systems converged, indicating stable conformational dynamics of AURKB (Fig. 2C).

Solvent accessible surface area (SASA) is a quantitative measurement that correlates the molecular surface area of protein accessible to solvent molecules and provides information about the extent of protein and solvent interaction. SASA indicates the overall stability and protein folding with ligands. Higher SASA values suggest protein unfolding and a decrease in stability score. Average SASA values for native AURKB and complexed with noscapine calculated during 100 ns MD simulation were 152.93 nm^2 and 170.09 $nm^{2,}$ respectively. The slight increment in SASA might arise due to conformational changes in the internal residues of protein upon ligand binding. These structural alterations expose the protein residues to the solvent. However, significant differences were not observed in SASA findings between both systems, suggesting stable structural dynamics of the protein (Fig. 2D). The details of trajectories are provided in Table 3.

Table 3
Calculated parameters of native AURKB and AURKB complex with noscapine obtained after 100 ns simulation.

System	RMSD (nm)	RMSF (nm)	*Rg* (nm)	SASA (nm^2)	#H-bonds
AURKB	0.44	0.16	1.94	152.93	198
AURKB-Noscapine	0.43	0.21	2.09	173.09	191

3.4. Hydrogen bonding analysis

Hydrogen bonding confers rigidity to protein and provides specificity to molecular interactions with ligands. Intramolecular hydrogen bonding confers secondary and tertiary structural integrity to protein. To determine and authenticate the stability of free AURKB and AURKB complex docked with noscapine, the hydrogen bonds paired within 3.5Å in the solvent environment were calculated during 100 ns MD simulation. The average number of hydrogen bonds found within AURKB and after noscapine binding were 198 and 191, respectively. The negligible increase in intramolecular hydrogen bonds before and after binding could indicate compactness in protein structure upon ligand interaction. The plots generated did not show significant deviations in hydrogen bonds in AURKB after noscapine binding. The findings suggest stable complex formation throughout the simulation (Fig. 3A).

3.5. Secondary structural changes

Secondary structure changes upon ligand binding were observed as a function of time. To estimate the secondary structural content of free and complexed AURKB, parameters including α-helix, β-sheet, and turns were plotted throughout the simulation process. Based on the analysis, the average number of residues forming coils and bends decreased in the AURKB-noscapine complex. Overall, the average residues involved in forming major secondary structures, including *α*-helix and *β*-turns, were increased in the AURKB-noscapine docked structure (Table 4). In conclusion, no significant divergence in the

secondary structural content of both systems was observed, indicating the possibility of stable complex formation (Figs. 3B and 3C).

Table 4
Residues participating in average structure formation.

Secondary structure	AURKB	AURKB-Noscapine
Coil	81	78
β-sheet	37	40
β-bridge	4	3
Bend	30	27
Turn	24	26
α-helix	94	97
π-helix	0	0
3_{10}-helix	5	4

3.6. Principal component analysis of free energy landscape

Essential dynamics or principal component analysis was conducted to elucidate the overall expansion of protein conformation during simulation. PCA is a well-defined mathematical methodology to deduce global and co-related motions of a protein in atomic simulation characterized by eigenvectors. PCA analysis reveals the average motion of protein, exposing structures underlying nuclear fluctuations. The sum of eigenvectors indicates total motility in the system and compares the extent of total protein flexibility under different conditions. A set of eigenvectors and eigenvalues were projected because of PCA analyses. A cluster of stable conformation reveals that the noscapine-bound form of AURKB occupies a larger conformational space than the free AURKB. These findings indicate slightly higher structural stability in the free AURKB form than the noscapine bound form (Fig. 4A and 4B).

Free energy landscapes were also plotted to gain insights into protein folding pattern differences upon noscapine binding. To compare the conformational behavior of both systems, the first two eigenvectors were used to explore the Gibbs free energy landscape. The binding of noscapine to the active pocket of AURKB showed progression of 3–4 global minima, indicating distinct differences in the projection of free energy with energetically favored and relatively stable conformation of free AURKB as compared to noscapine bound complex. Such changes suggest that the binding of noscapine slightly perturbs AURKB structural conformation, eventually attenuating enzyme activity (Figs. 4C and 4D).

3.7. Expression and purification of recombinant AURKB

Recombinant 6X-Histidine tag-AURKB was expressed in *E. coli* cells (BL21) and purified from IBs fraction. Purified AURKB protein showed a single band of approximately 37.5 kDa in SDS-PAGE. UV-Spectra

analysis recorded in the 240–340 nm range showed properly folded protein without aggregation. Additionally, purified AURKB was subjected to fluorescence analysis by excitation at 280 nm, and emission was measured in the 300–400 nm range. Both absorption spectra and fluorescence analysis of AURKB did not show any conformational changes or aggregation in purified AURKB protein. Later, the enzymatic activity of pure AURKB was detected using ATPase assay. ATPase assay of purified AURKB showed complete hydrolysis of ATP (200 μM), and beyond this, ATP concentration saturation in catalytic activity was noted.

3.8. Fluorescence binding studies

The binding affinity obtained from molecular docking was validated through fluorescence spectroscopy conducted on native AURKB. Adding noscapine in a dose-dependent manner (1–50 μM) in purified AURKB (4 μM) caused alteration in the fluorophore microenvironment, leading to fluorescence quenching of native AURKB. AURKB quenching fluorescence spectra were plotted against increasing concentrations of noscapine (Fig. 5A). The binding constant was estimated from changes in fluorescence intensity upon noscapine titration. As represented in the Stern-Volmer plot, increasing the concentration of noscapine showed an inverse co-relationship with the fluorescence intensity of AURKB (Fig. 5B). The binding affinity of noscapine was found to be 1.4×10^{4} M^{-1}.

3.9. Kinase inhibition assay

The findings of *in-silico* studies suggested that noscapine binds AURKB with strong affinity, and several interactions stabilize the complex. The inhibitory potential of noscapine was estimated using ATPase assay in a dose-dependent manner. The assay was carried out on recombinant AURKB (4 μM) protein with increasing concentration of noscapine (0-100 μM). Results of the kinase assay revealed that noscapine inhibited AURKB activity in a concentration-dependent manner. A decrease in AURKB activity was plotted as a function of percent inhibition with increasing ligand concentration using the formula 100- (A/ Å ×100), where A and A^{0} depict enzyme activities of AURKB in the presence and absence of ligand, respectively [31]. The IC_{50} of noscapine was calculated using AAT Bioquest software and was found to be 26.6 μM. An inverse co-relationship of loss of AURKB activity with increasing noscapine concentration was observed (Fig. 5C). Noscapine might interact with the ATP binding pocket of AURKB located in the N-terminal domain, thereby reducing the accessibility of the ATP substrate.

3.10. Cell viability studies

Overexpressed AURKB exhibits oncogenic characteristics by facilitating cancer cell growth and viability. Since AURKB is a vital cell cycle regulator, an aberrant phosphorylation pattern might trigger cancer cell development. As documented in previous studies, AURKB hyperexpression plays a prominent role in lung cancer. Therefore, the effects of noscapine treatment on A549 cell viability were investigated. A549 and HEK293 were exposed to different concentrations of noscapine (0-250 μM) for 48 hrs and later collected for MTT assay. Cell viability assay results depicted enhanced A549 cell death upon noscapine exposure in a concentration-dependent manner. Interestingly, cytotoxic effects of noscapine were not observed in

HEK293 cells. The observed IC_{50} of noscapine was assessed using a cell growth curve and found to be 68.4 μM. These results suggested that noscapine decreased cancer cell viability and did not show considerable cytotoxicity against HEK293 cells (Fig. 6A). The observations of the cell viability test were consistent with the previous reports stating that AURKB inhibition decreases cancer cell proliferation [32].

3.11. Cell apoptosis analysis

Apoptosis is essential for controlling cell growth in a normal state. However, cancer cells show deviation from normal pathways, thus evading apoptosis and dividing uncontrollably. AURKB overexpression has a significant role in several cancerous cells' growth and apoptotic evasion. Therefore, this study evaluated the apoptotic effects of noscapine treatment on cancer cells via possible AURKB inhibition. A549 cancer cells were exposed to an IC_{50} dose of noscapine (68.4 μM) for 48 hrs and later harvested and processed for apoptosis induction by annexin-V staining. Treated cells were fixed, stained, and analyzed with the flow cytometry technique. The observations revealed that noscapine triggered apoptosis in 33% of A549 cells compared to untreated control cells. These results suggested that inhibition of AURKB using noscapine exhibits apoptotic effects on A549 cells and induces apoptosis. The findings also revealed that most A549 cells (31.2%) post noscapine treatment for 48 hrs at IC50 entered the early apoptotic phase. Interestingly, a very low percentage of untreated A549 cells entered apoptosis (Figs. 6B and 6C).

3.12. DAPI staining

Nuclear morphology of A549 cells treated with IC_{50} concentration of noscapine compared to untreated control was observed through 4',6-diamidino-2-phenylindole (DAPI) staining. Due to its high affinity for nuclear DNA, DAPI is frequently used to analyze drug-induced changes in nuclear morphology [33]. Apoptosis is documented for inducing changes in nuclear morphology, where the condensation of chromatin and the fragmentation of the nucleus serve as potential indicators for detecting these altered atomic features. The nuclear alteration taking place throughout apoptosis induced by IC_{50} concentration of noscapine compared to untreated control cells is depicted in Figs. 7A, 7B, and 7C. The result showed a good correlation with flow cytometry data, confirming the efficacy of noscapine. Our findings align with existing literature, which associates nuclear alterations observed during DAPI staining with specific cellular apoptosis processes [26].

3.13. Wound healing assay

Abnormal migration is a hallmark feature of cancer cells with metastatic potential. A wound-healing assay was conducted to determine the anti-migrating effects of noscapine treatment on A549 cells. The findings revealed suppressive effects of noscapine on cancer cell migration compared with untreated cells. The results provide evidence of the possible role of noscapine in combating metastatic potential in A549 cells (Figs. 7D and 7E).

4. Discussion

Lung cancer has been the leading cause of mortality globally for decades [34]. Aberrant functioning of several signaling cascades due to poor or over-expression has been the prime underlying cause of human malignancies. Altered expression levels of human protein kinases acting as downstream and upstream molecules controlling phosphorylation events have been reported to trigger cancer initiation and progression [35]. Considering the pivotal role of these kinases in cancer pathogenesis, therapeutic targeting of these key signaling modulators has been a top-notch choice of pharmacological industries and researchers to combat cancer. After G-protein coupled receptors, kinase is the second major targeted group in cancer interventional strategies.

To date, 37 kinase inhibitors have been FDA-approved and implemented in therapeutic breast and lung cancer regimes, whereas 150 inhibitors are in different phases of clinical trials [36]. Although several anti-cancer drugs from both synthetic and natural origins are exploited in cancer treatment, they are associated with the non-selective killing of tumor cells. Therefore, attenuating distinct signaling pathways can be less toxic to non-cancerous cells, improving prognosis. Human AURKB belongs to the serine/threonine kinase family, which controls microtubule assembly formation during mitosis. AURKB targets include Survivin, Borealin, Histone B, and p53 protein. Aberrant activity of AURKB results in the accumulation of genetic material, thereby causing aneuploidy and genetic mutations. In previous studies, AURKB overexpression has been reported in lung carcinoma, and its targeted mitigation caused clinical remission of cancer [37]. Studies on selective AURKB targeting with in-depth molecular understanding are still elusive. Although synthetic inhibitors of AURKB, including volasertib, alisertib, and alisertib, have been FDA-approved [38], inhibitors from natural sources have not been extensively explored.

Until now, chemotherapy has been widely accepted as a conventional anti-cancer therapy, but long-term exposure poses serious threats to patients. Hence, the implication of alternative therapy with high clinical efficacy and safety for non-cancerous cells is deemed essential. Dietary phytochemicals possess anti-oxidative and anti-inflammatory features and have been reported to combat uncontrolled cell proliferation and metastasis via attenuation of signaling cascades. Preclinical studies have documented that several phytochemicals attenuated dysfunctioned human kinases, including Sphk1, MARK4, Cdk6/5, GSK3β, MAPK, and Raf, significantly reversing cancer cell progression [38–40]. However, the underlying mechanism has not been completely explored.

Noscapine has been an attractive anti-mitotic lead compound that is reported to destabilize microtubule assembly, leading to programmed cell death, the process in which AURKB plays an important role. Noscapine action was similar to paclitaxel and colchicine, i.e., binding to tubulin in mitotic cells, though at different sites [41]. Therefore, this study investigated the AURKB inhibitory potential of noscapine, a dietary polyphenol, and elucidated structural changes, binding mechanisms, and interaction patterns with AURKB using high-throughput screening tools.

Molecular docking revealed that noscapine occupied an active pocket of AURKB with a binding energy of -7.4 kcal/mol with several non-covalent interactions. The findings of molecular docking were validated with fluorescence spectroscopy that showed significant quenching of native AURKB and high binding

affinity upon dose-dependent exposure to noscapine. The inhibitory potential of noscapine was investigated using a malachite green assay in a concentrated dependent manner on recombinantly expressed full-length AURKB. It was observed that noscapine exposure abrogated AURKB catalytic activity in the micromolar range. As evidenced by molecular docking analysis, noscapine interacted with important residues of the active pocket of AURKB, including Lys106, which possibly explains noscapine-mediated AURKB inhibition in vitro. Our findings align with a recent study stating noscapine mediated inhibition of tyrosine kinase activity epidermal growth factor receptor in osteosarcoma [19].

Molecular docking and kinase inhibition assay results depict that noscapine might act as a competitive inhibitor of ATP substrate and downregulate AURKB activity. Further, to gain atomic insights into structural changes upon noscapine binding, simulation studies of native AURKB and AURKB-noscapine complexes were also performed for 100 ns. Slight non-significant changes in simulation trajectories (RMSD, RMSF, *Rg*, SASA) of the AURKB-noscapine complex compared with free were noted. These inevitable random fluctuations might result from the initial repositioning of noscapine in the active cavity of AURKB, and the system attained stability. Similarly, no significant conformational changes in secondary structures were observed in the AURKB-noscapine complex throughout the simulation process. The findings indicate that noscapine strongly occupies the binding site in AURKB and does not trigger major structure perturbations overall.

Noscapine has established a broad pharmacological role due to its anti-oxidant, anti-inflammatory, and anti-cancerous properties [42]. Cell cytotoxicity assay was performed on lung cancer cell lines (A549) and normal cells (HEK293). The observations of the MTT assay indicated a strong anti-proliferative action of noscapine on A549 cells in a dose-dependent manner. In contrast, HEK293 cells were feebly affected upon noscapine treatment. Additionally, anti-apoptotic features of noscapine were monitored with flow cytometry. The findings stated that a significant percentage of A549 cells entered early apoptosis upon noscapine exposure compared to untreated cells, depicting its strong anti-apoptotic potential. In a recent study, noscapine induced apoptosis in various breast cancer cell models *via* inducing *Bax* gene expression, reducing *Bcl-2* expression [43].

Also, noscapine triggered morphological changes in the cell nucleus by chromosomal condensation and nuclear fragmentation, as evident through nuclear staining. Noscapine has reported affinity with tubulin protein that could decrease disturbed microtubule assembly, causing aneuploidy [44]. Certain outcomes from previous literature have postulated noscapine-based reduction of endothelial cell migration in different cancer types [19, 42]. Similarly, the wound healing assay results in this study revealed significantly reduced A549 cell migration and motility upon noscapine exposure compared to untreated cells. It can be stated that noscapine exhibited anti-proliferative and anti-metastatic potential on A549 cells. Cell-based studies substantiate that noscapine can be considered a potential anti-cancerous compound with a multifaceted role and fewer side effects on healthy cells.

Furthermore, the observations of *in-silico* studies support that noscapine might reduce ATP accessibility of AURKB by occupying an active pocket and attenuating catalytic potential. Nevertheless, the study

outcomes provide deeper insights into designing newly inspired advanced noscapine derivatives as therapeutic agents against several life-threatening diseases. Therefore, a noscapine scaffold with required modification can be exploited to develop therapeutic anti-cancer agents with enhanced efficacy and potency.

5. Conclusions

Recent advancements in decoding fundamental molecular mechanisms underlying aberrant cancer cell signaling have elucidated the critical role of human protein kinases in the oncogenesis and metastasis of various cancers. Kinase inhibitors signify targeted therapy consequential to understanding underlying molecular genetics and signaling cascades. Many FDA-approved kinase inhibitors target ATP binding pocket of kinases and display therapeutic indications against oncogenesis. The pathological role of constitutively hyper-expressed AURKB in lung carcinoma has been well documented in the literature. Overactive AURKB in mitotic cells accounts for abnormal chromosomal shuffling and genetic aneuploidy, leading to cancer cell formation. In addition, conventional treatment strategies are non-specific, causing damage to healthy cells. Therefore, modulation of AURKB activity using potent inhibitors could be an attractive strategy in combating AURKB-associated cancers, including lung cancers. With the growing understanding of the structure-activity relationship and high throughput screening tools, we first discovered noscapine binding to the ATP binding pocket of AURKB. Cell-based studies also supported noscapine's anti-proliferative, anti-apoptotic, and anti-metastatic characteristics. The present findings support the conception that noscapine may offer a novel therapeutic strategy against lung carcinoma, but these results warrant further testing.

Abbreviations

ATP: Adenosine-tri phosphate, AURKB: Aurora kinase B, A549: DAPI, 4',6-diamidino-2-phenylindole; Human alveolar basal epithelial cells, HEK293: Human embryonic kidney cells, DMEM: Dulbecco's modified eagle medium, EMT: Epithelial to mesenchymal transition, FBS: Fetal bovine serum, IBs: Inclusion bodies, IC_{50}: Half-maximal inhibitory concentration, Ni-NTA: Nickel-nitrilotriacetic acid chromatography, MD: Molecular dynamics, μM: Micromolar, mM: Millimolar, MTT: 3-[4,5-dimethylthiazol-2-yl]-2,5 diphenyl tetrazolium bromide, PASS: Prediction of activity spectra for substances, PI, Propidium iodide; *Rg*: Radius of gyration, RMSD: Root mean square deviation, RMSF: Root mean square frequency, SASA: Solvent accessible surface area.

Declarations

Funding: This work is supported by grants from the Department of Health and Research, Government of India (Grant No.R.12014/60/2022-HR).

Acknowledgments

SN and MIH thank the Department of Health and Research, Government of India, for the award of the Young Scientist Fellowship (Grant No. R.12014/60/2022-HR).

Data availability statement

All data generated or analyzed during this study are included in this published article.

Compliance with ethical standards

Conflict of interest: The authors declare no conflict of interest.

Research involving Human Participants and Animals: N/A

Informed consent: N/A

References

1. R. Kannaiyan, D. Mahadevan, Expert review of anticancer therapy 18 (2018) 1249.
2. E.A. Nigg, Nature reviews Molecular cell biology 2 (2001) 21.
3. S.L. McVey, J.K. Cosby, N.J. Nannas, International Journal of Molecular Sciences 22 (2021) 8818.
4. C. Crosio, G.M. Fimia, R. Loury, M. Kimura, Y. Okano, H. Zhou, S. Sen, C.D. Allis, P. Sassone-Corsi, Molecular and cellular biology 22 (2002) 874.
5. L. Wu, C.A. Ma, Y. Zhao, A. Jain, Journal of Biological Chemistry 286 (2011) 2236.
6. N. Jelluma, A.B. Brenkman, N.J. van den Broek, C.W. Cruijsen, M.H. van Osch, S.M. Lens, R.H. Medema, G.J. Kops, Cell 132 (2008) 233.
7. N.A. Borah, M.M. Reddy, Molecules 26 (2021) 1981.
8. A.K. Shaalan, T.H. Teshima, A.S. Tucker, G.B. Proctor, Cell Death Discovery 7 (2021) 16.
9. B.A. Helfrich, J. Kim, D. Gao, D.C. Chan, Z. Zhang, A.-C. Tan, P.A. Bunn Jr, Molecular cancer therapeutics 15 (2016) 2314.
10. R.K. Tyler, N. Shpiro, R. Marquez, P.A. Eyers, Cell cycle 6 (2007) 2846.
11. M. Yousuf, A. Shamsi, A. Queen, M. Shahbaaz, P. Khan, A. Hussain, M.F. Alajmi, Q.M. Rizwanul Haque, M. Imtaiyaz Hassan, Journal of Cellular Biochemistry 122 (2021) 897.
12. L. Wu, J. Li, T. Liu, S. Li, J. Feng, Q. Yu, J. Zhang, J. Chen, Y. Zhou, J. Ji, Cancer medicine 8 (2019) 4806.
13. D. Liang, F. Li, Y. Fu, Y. Cao, X. Song, T. Wang, W. Wang, M. Guo, E. Zhou, D. Li, Inflammation 37 (2014) 214.
14. C. Qi, X. Wang, Z. Shen, S. Chen, H. Yu, N. Williams, G. Wang, Cell research 28 (2018) 544.
15. F. Nemati, I. Bischoff-Kont, P. Salehi, S. Nejad-Ebrahimi, M. Mohebbi, M. Bararjanian, N. Hadian, Z. Hassanpour, Y. Jung, S. Schaerlaekens, Bioorganic Chemistry 115 (2021) 105135.

16. R. Tomar, A. Sahni, I. Chandra, V. Tomar, R. Chandra, Mini-Reviews in Organic Chemistry 15 (2018) 345.
17. M.B. Chougule, A.R. Patel, T. Jackson, M. Singh, PloS one 6 (2011) e17733.
18. M.B. Chougule, A. Patel, P. Sachdeva, T. Jackson, M. Singh, PLoS one 6 (2011) e27394.
19. M. He, L. Jiang, Z. Ren, G. Wang, J. Wang, Scientific Reports 6 (2016) 37062.
20. M.A. Altinoz, G. Topcu, A. Hacimuftuoglu, A. Ozpinar, A. Ozpinar, E. Hacker, İ. Elmaci, Neurochemical research 44 (2019) 1796.
21. B. Sung, K.S. Ahn, B.B. Aggarwal, Cancer research 70 (2010) 3259.
22. N. Singh, S. Singh, S. Sewariya, A. Singh, G. Rathee, D. Sood, N. Kumar, I. Chandra, S.K. Dass, V. Tomar, Organic & Medicinal Chemistry International Journal 9 (2019) 48.
23. R. Aneja, S. Asress, N. Dhiman, A. Awasthi, P.C. Rida, S.K. Arora, J. Zhou, J.D. Glass, H.C. Joshi, International journal of cancer 126 (2010) 256.
24. T. Mohammad, Y. Mathur, M.I. Hassan, Briefings in Bioinformatics 22 (2021) bbaa279.
25. S. Noor, A. Choudhury, A. Raza, A. Ashraf, K.U. Islam, A. Hussain, K. Imtiyaz, A. Islam, M.I. Hassan, Int J Biol Macromol 258 (2024) 128813.
26. J.R. Eidet, L. Pasovic, R. Maria, C.J. Jackson, T.P. Utheim, Diagnostic pathology 9 (2014) 1.
27. M. Voura, P. Khan, S. Thysiadis, S. Katsamakas, A. Queen, G.M. Hasan, S. Ali, V. Sarli, M.I. Hassan, Scientific Reports 9 (2019) 1676.
28. A. Queen, P. Khan, D. Idrees, A. Azam, M.I. Hassan, International journal of biological macromolecules 106 (2018) 840.
29. K.U. Islam, S. Anwar, A.A. Patel, M.T. Mirdad, M.T. Mirdad, M.I. Azmi, T. Ahmad, Z. Fatima, J. Iqbal, Viruses 15 (2023) 464.
30. P. Khan, A. Queen, T. Mohammad, Smita, N.S. Khan, Z.B. Hafeez, M.I. Hassan, S. Ali, Journal of natural products 82 (2019) 2252.
31. S. Roy, T. Mohammad, P. Gupta, R. Dahiya, S. Parveen, S. Luqman, G.M. Hasan, M.I. Hassan, ACS omega 5 (2020) 21550.
32. C. Wang, J. Chen, W. Cao, L. Sun, H. Sun, Y. Liu, European journal of pharmacology 779 (2016) 1.
33. S. Sikdar, A. Mukherjee, N. Boujedaini, A.R. Khuda-Bukhsh, CELLMED 3 (2013) 9.1.
34. J.A. Barta, C.A. Powell, J.P. Wisnivesky, Annals of global health 85 (2019).
35. L. Zhong, Y. Li, L. Xiong, W. Wang, M. Wu, T. Yuan, W. Yang, C. Tian, Z. Miao, T. Wang, Signal transduction and targeted therapy 6 (2021) 201.
36. K.S. Bhullar, N.O. Lagarón, E.M. McGowan, I. Parmar, A. Jha, B.P. Hubbard, H.V. Rupasinghe, Molecular cancer 17 (2018) 1.
37. S. Smith, N. Bowers, D. Betticher, O. Gautschi, D. Ratschiller, P. Hoban, R. Booton, M. Santibanez-Koref, J. Heighway, British journal of cancer 93 (2005) 719.
38. A. Rivera Rivera, L. Castillo-Pichardo, Y. Gerena, S. Dharmawardhane, PLoS One 11 (2016) e0157251.

39. X. Yan, M. Qi, P. Li, Y. Zhan, H. Shao, Cell & bioscience 7 (2017) 1.
40. C. Spagnuolo, G.L. Russo, I.E. Orhan, S. Habtemariam, M. Daglia, A. Sureda, S.F. Nabavi, K.P. Devi, M.R. Loizzo, R. Tundis, Advances in nutrition 6 (2015) 408.
41. M. Mahmoudian, P. Rahimi-Moghaddam, Recent patents on anti-cancer drug discovery 4 (2009) 92.
42. P. Rahmanian-Devin, V. Baradaran Rahimi, M.R. Jaafari, S. Golmohammadzadeh, Z. Sanei-Far, V.R. Askari, Evidence-based Complementary and Alternative Medicine 2021 (2021).
43. N. Heidari, B. Goliaei, P.R. Moghaddam, N. Rahbar-Roshandel, M. Mahmoudian, Anti-cancer drugs 18 (2007) 1139.
44. K. Ye, Y. Ke, N. Keshava, J. Shanks, J.A. Kapp, R.R. Tekmal, J. Petros, H.C. Joshi, Proceedings of the National Academy of Sciences 95 (1998) 1601.

Figures

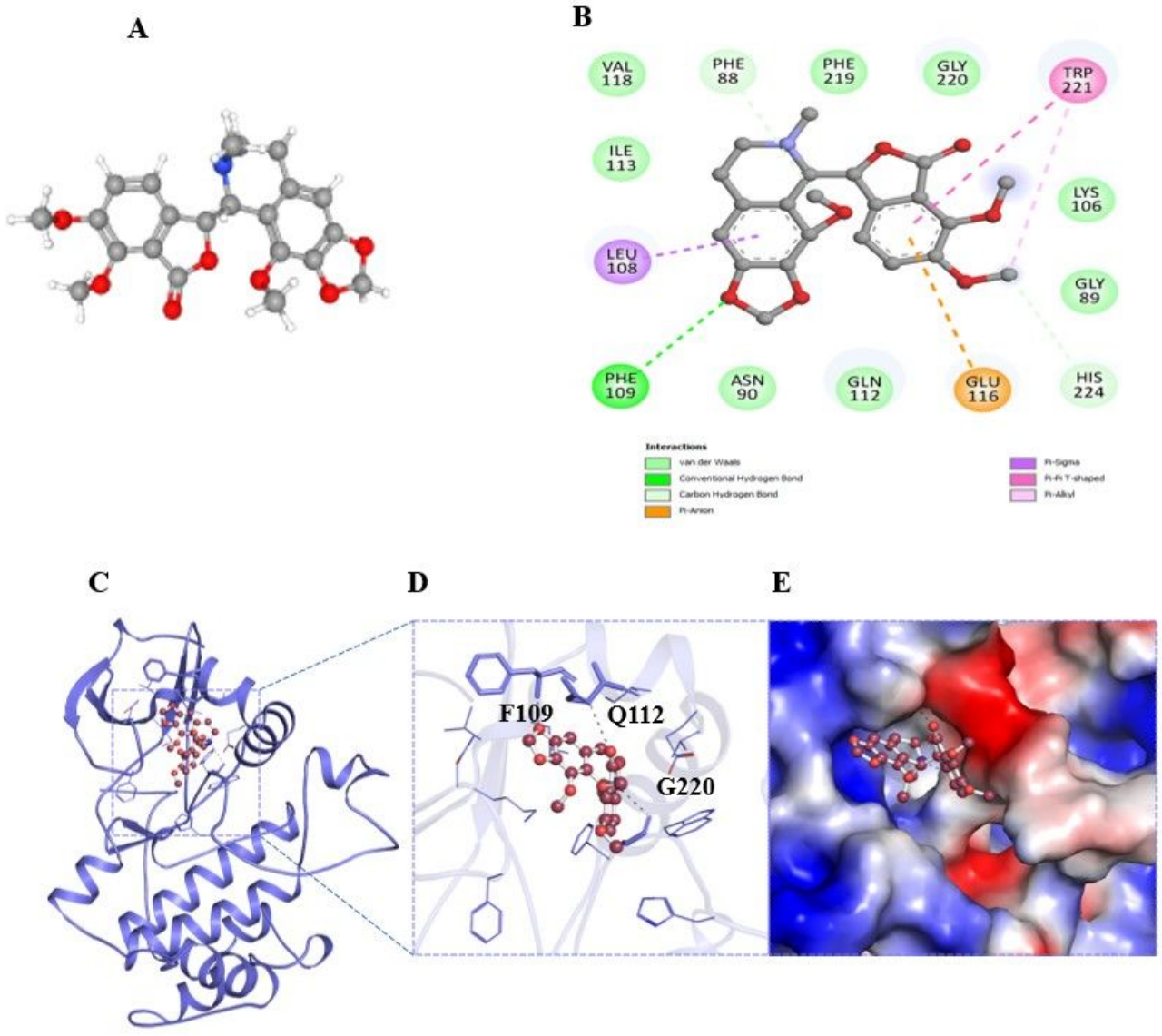

Figure 1

Structural representation of AURKB in-complex with noscapine. (A) 3D structure of noscapine, **(B)** 2D representation of AURKB residues interacting to noscapine, **(C)** Showing overall structure of AURKB in-complex with noscapine **(D)** 3D interaction of noscapine with active-site pocket of AURKB, **(E)** Surface electrostatic potential view of AURKB binding pocket with noscapine.

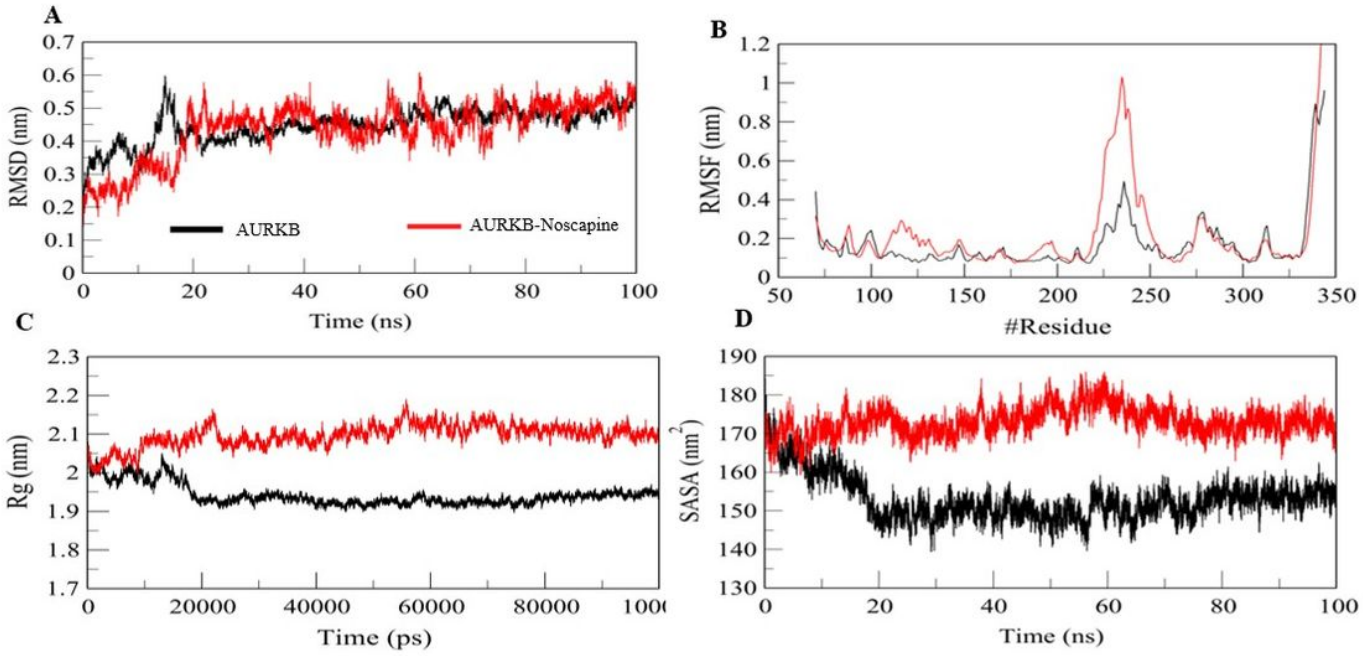

Figure 2

Structural dynamics of free AURKB upon binding of noscapine. (A) RMSD plot of free AURKB as a function of time with noscapine, (B) RMSF plot of free AURKB and upon binding with noscapine, (C) Time evolution of radius of gyration, (D) SASA plot of free AURKB as a function of time.

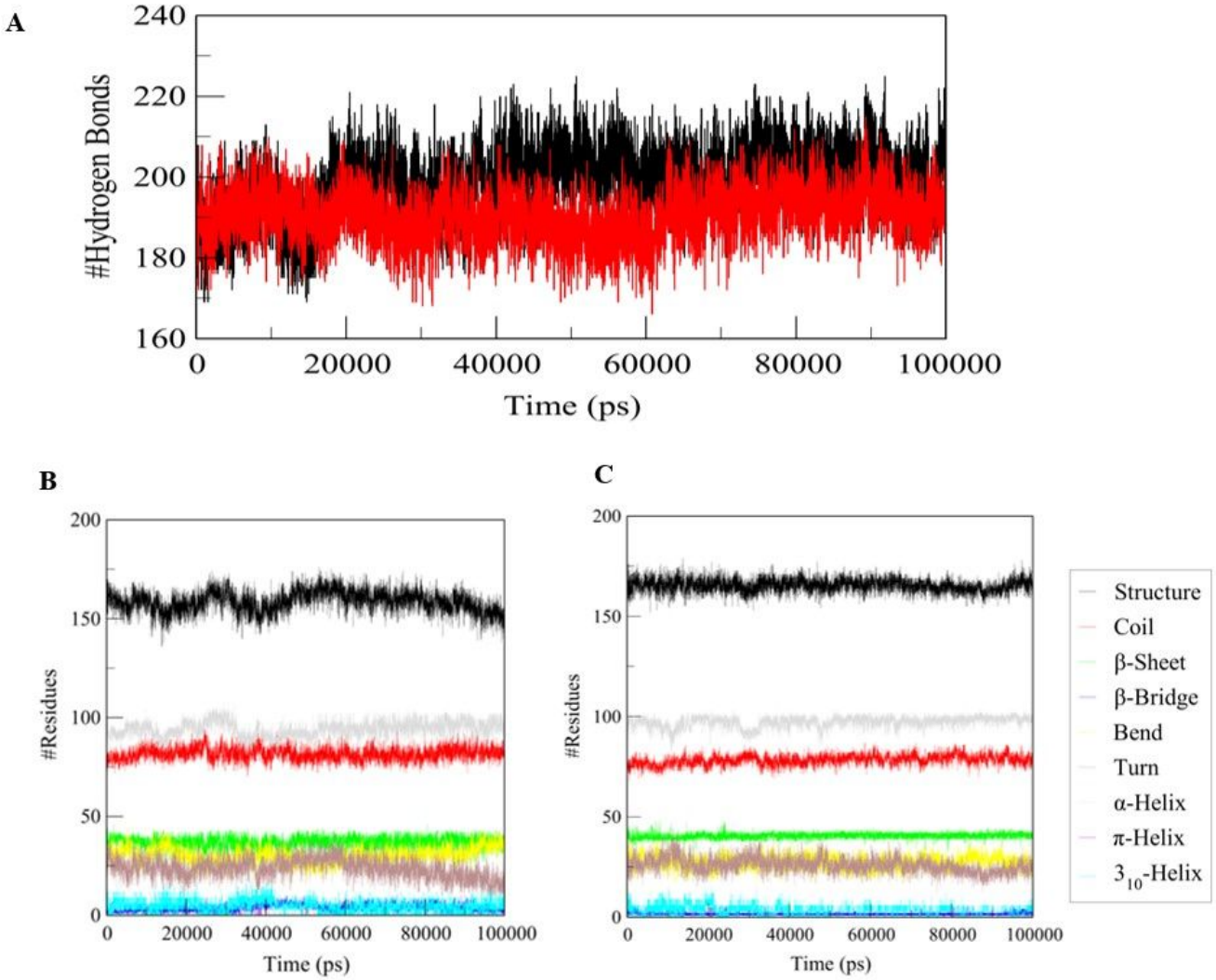

Figure 3

Time evolution and stability pattern of hydrogen bonds formed, (A) Intra-molecular hydrogen bonds within the AURKB structure upon noscapine binding. Secondary structure content of (B) free -AURKB, (C) AURKB-noscapine complex *Structure ¼ α-helix + β-sheet + β-bridge + turn.

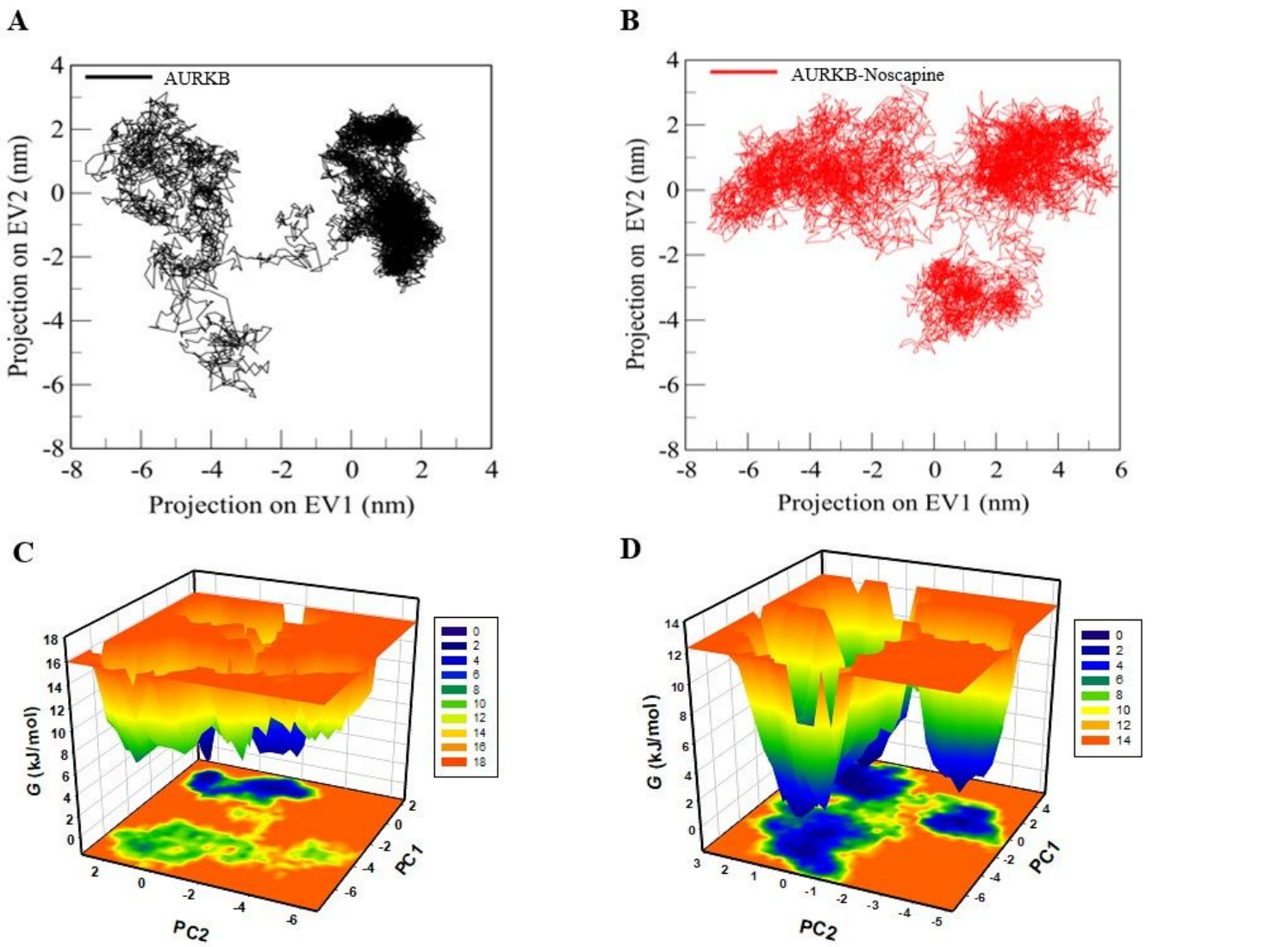

Figure 4

Principal component analysis. 2D projections of trajectories on eigenvectors showing different projections of (A) free-AURKB, (B) AURKB-noscapine. Gibbs free energy landscape generated by projecting the principal components, PC1 and PC2 during MD simulation (C) free- AURKB, (D) AURKB-noscapine.

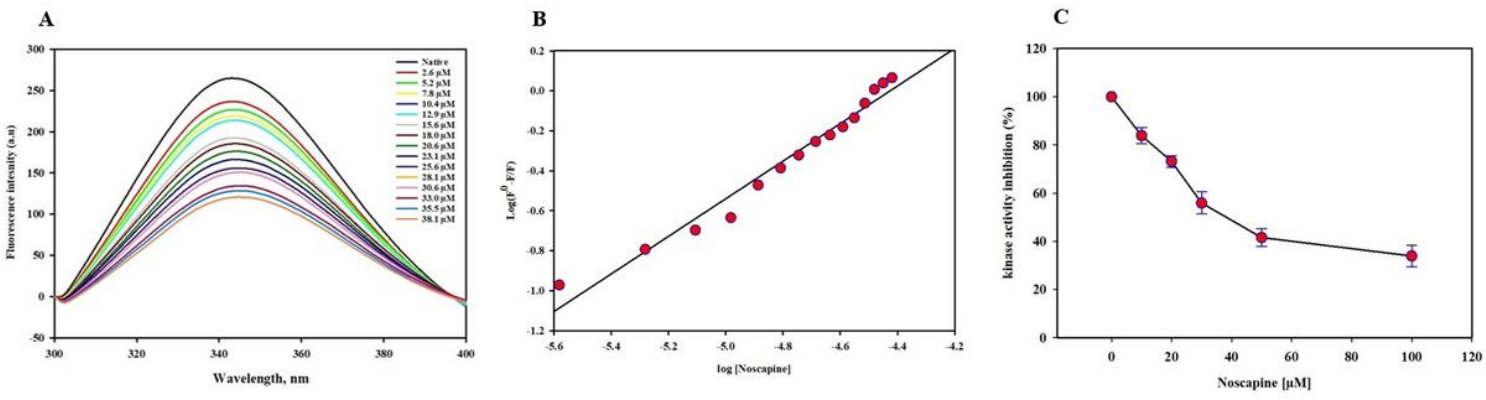

Figure 5

Binding studies of AURKB with noscapine (A) Fluorescence emission spectra of AURKB with increasing concentration of noscapine, (B) Stern-Volmer plot of noscapine binding with AURKB. **(C)** ATPase inhibition assay depicting the effect noscapine on AURKB kinase activity.

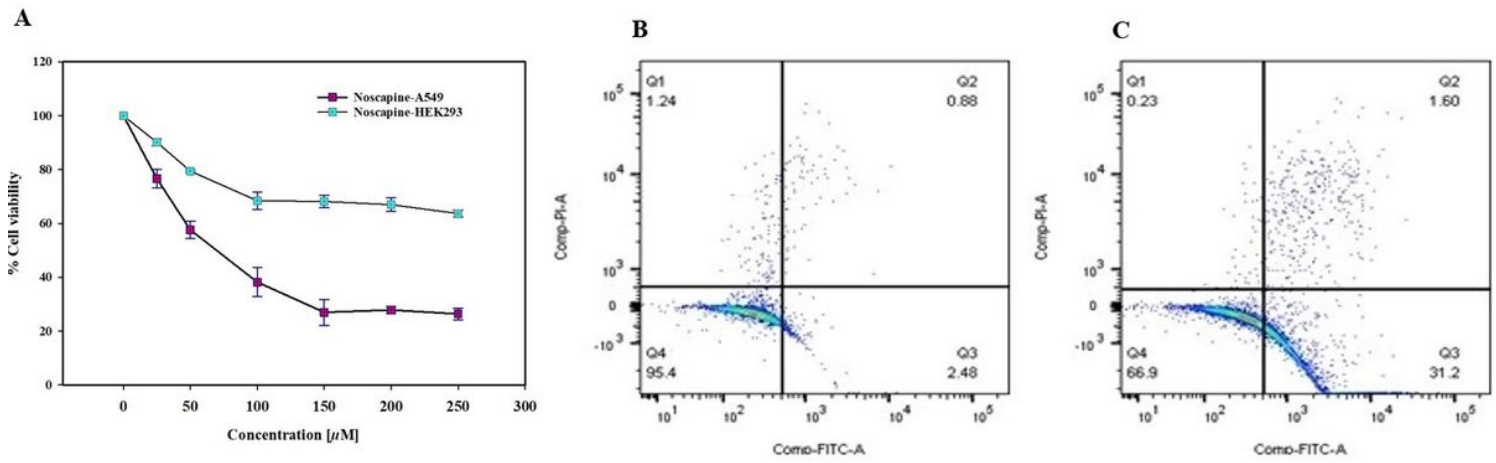

Figure 6

(A) Cell viability assay of noscapine on lung cancer cells (A549) and normal cells (HEK-293) Each cell type was treated with increasing concentration of noscapine (0-250 μM) for 48 hrs. Cell viability percentage (%) was calculated with respect to untreated cells. Typical quadrant analysis of Annexin V-FITC/PI staining flow cytometry conducted on (B) untreated and (C) A549 cells treated with noscapine for 48 hrs. The percentage of cells (%) is shown in each quadrant. The proportion of viable cells are depicted in Q4 quadrant (FITC-/PI-), early apoptotic cells in Q3 quadrant (FITC+/PI-), late apoptotic cells in Q2 quadrant (FITC+/PI+), and necrotic cells (FITC-/PI+).

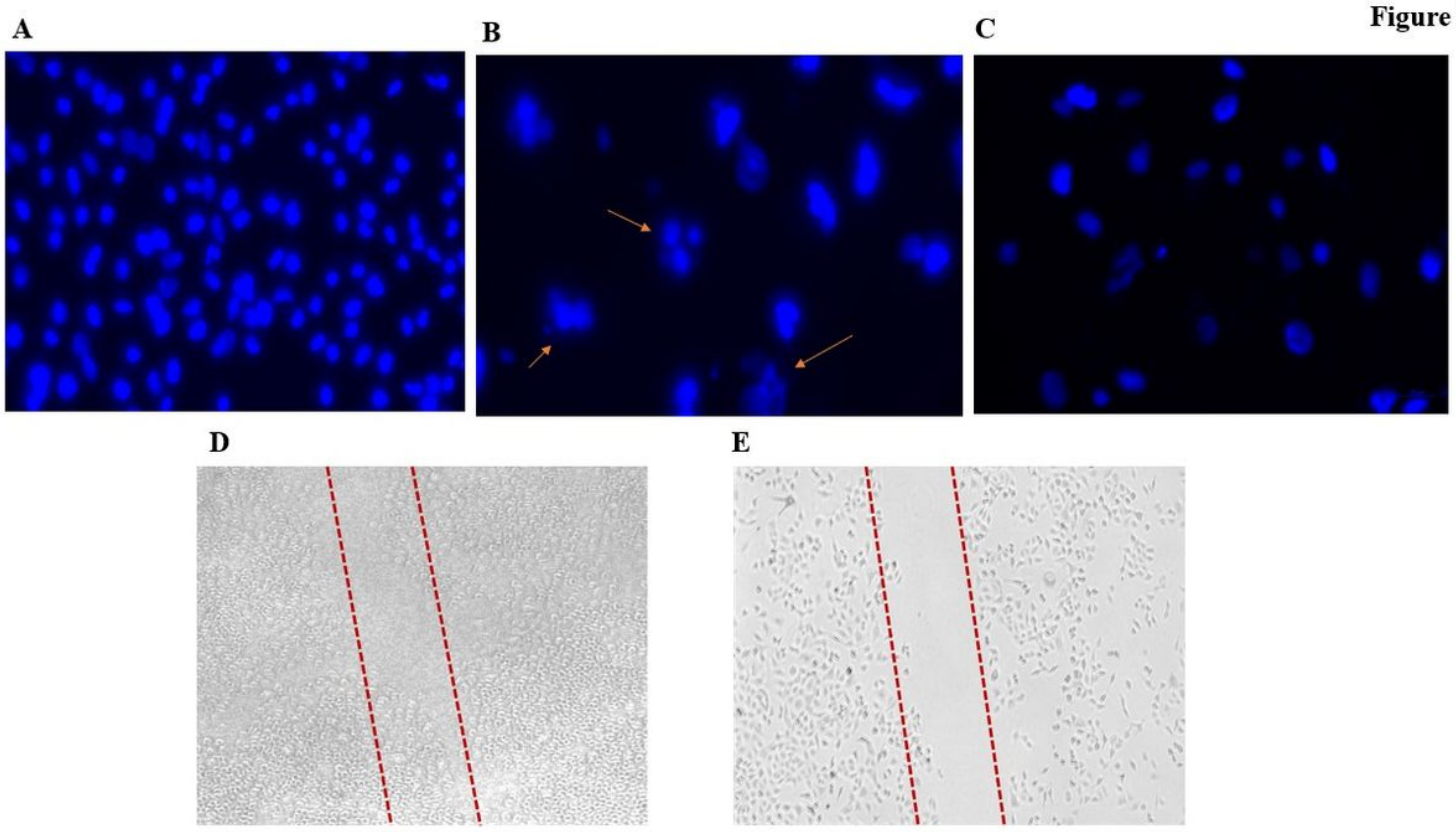

Figure 7

DAPI staining of A549 cells treated with IC50 concentration of noscapine (A) untreated cells, (B) noscapine (C) Starosporin. The red arrows indicate apoptotic cells. Cells were treated with the IC_{50} concentration of noscapine for 48 hrs Representative images (10X original magnification) (D) untreated cells, (E) noscapine treated cells showing inhibition of A549 cell migration as determined by the wound healing assay.